JOURNAL OF MATERIALS SCIENCE 35 (2000) 1153–1164

Microstructural evolution of Hi-Nicalon™ SiC fibers annealed and crept in various oxygen partial pressure atmospheres

G. W. HE, T. SHIBAYAMA, H. TAKAHASHI
Center for Advanced Research of Energy Technology, Hokkaido University, Kita-13, Nishi-8, Kita-Ku, Sapporo 060-8628, Japan

It is expected that in the future SiC fiber-reinforced ceramic-matrix composites (CMCs) will be used in high temperature and hostile environments. In this study, Hi-Nicalon™ SiC fibers were annealed and crept at 1500 °C for 1 hour in air, an argon flow and an ultra high-purity argon flow in order to investigate the effects of atmospheres and load conditions on the decomposition behavior and microstructural evolution of the fibers. After the fibers were annealed and crept in air, a silica layer with cracks was formed on the fiber surface. Under the creep load, the silica layer became thicker and porous due to the oxidation mechanism change from diffusion of ionic oxygen to transportation of oxygen molecules. An oxygen-enriched amorphous layer was formed at the fiber surface in the case of annealing in an argon flow, whereas SiC crystals were produced by the gas-phase reaction on the fiber surface when the fiber was crept in an argon flow. In an ultra high-purity argon flow, SiC crystals grew on the surface of both annealed and crept fibers. Growth of β-SiC grain was enhanced under low oxygen partial pressure atmospheres and creep load.

1. Introduction

In the future, it is expected that ceramic-matrix composites (CMCs) will be used in advanced gas turbine engines, aerospace planes and fusion reactors. In those applications, the composites will be used in corrosive combustion streams or ultra high vacuum environments under load conditions. The environmental durability of such composites is therefore a major concern. Thus, the responses of constituent materials (fiber, matrix and interface) to various environments must be clarified.

In 1975, small-diameter Si-C-O fibers were fabricated by deriving polycarbosilane (PCB) organic precursor and were named Nicalon [1, 2]. The weavability, high tensile strength and high Young's modulus of Nicalon fiber made it a potential candidate as a reinforcement material for ceramic. However, Nicalon fibers consist of SiC, free carbon and an amorphous silicon oxycarbide phase, resulting from the oxidation curing process. Nicalon fibers lose strength after exposure to temperatures of 1000 °C and above, due to decomposition of the silicon oxycarbide phase and coalescence of β-SiC [3–7]. New routes are being investigated to improve the thermal stability of ceramic fiber derived from organosilicon polymers. Okamura [8] developed a process to fabricate SiC fiber in which the curing of PCB is performed by electron beam irradiation in vacuum. Recently, fibers fabricated by this electron beam irradiation curing method are commercially available under the trade name Hi-Nicalon™. Studies using tensile tests, thermobalance measurement, scanning electron microscopy (SEM) observation, X-ray diffraction (XRD) and transmission electron microscopy (TEM) inspection have shown that Hi-Nicalon™ fibers have a very low oxygen content, excellent thermal stability characteristics and a greater creep resistant compared to Nicalon fibers [9–15]. Therefore, they are a prime candidate for reinforcing fiber in ceramic-matrix composites to be used under high temperature and hostile environments.

In the present work, the effects of environments and load conditions on the decomposition behavior and microstructural evolution of Hi-Nicalon™ fibers were investigated. Three kinds of atmospheres (oxygen content from 21% to 0.1 ppb) were employed for heating the Hi-Nicalon™ fibers under no load or under an applied load. The surface morphology and structural evolution of the fibers were studied by means of SEM, XRD and high-resolution transmission electron microscopy (HRTEM). The degradation behavior of fibers was also examined.

2. Experimental procedure

2.1. Materials

The Hi-Nicalon™ fibers used in this study (Lot. 225101, Nippon Carbon Inc, Japan) were obtained in the form of continuous yarn of approximately 500 single filaments. The average fiber diameter was 13 μm. The fibers were coated by a polyvinyl acetate sizing.

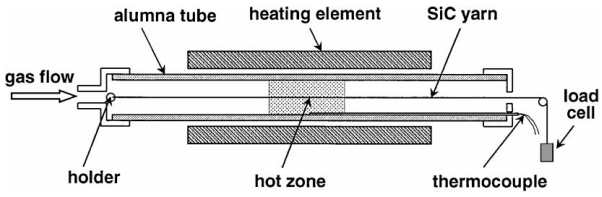

Figure 1 Schematic drawing of the apparatus for annealing and creep test.

The chemical compositions reported by the manufacturer are Si 62.4wt.%, C 37.1wt.%, and O 0.5wt.%.

2.2. Experimental methods

A horizontal furnace equipped with an SiC resistance heating element was employed, as schematically shown in Fig. 1. Annealing treatments and creep tests were

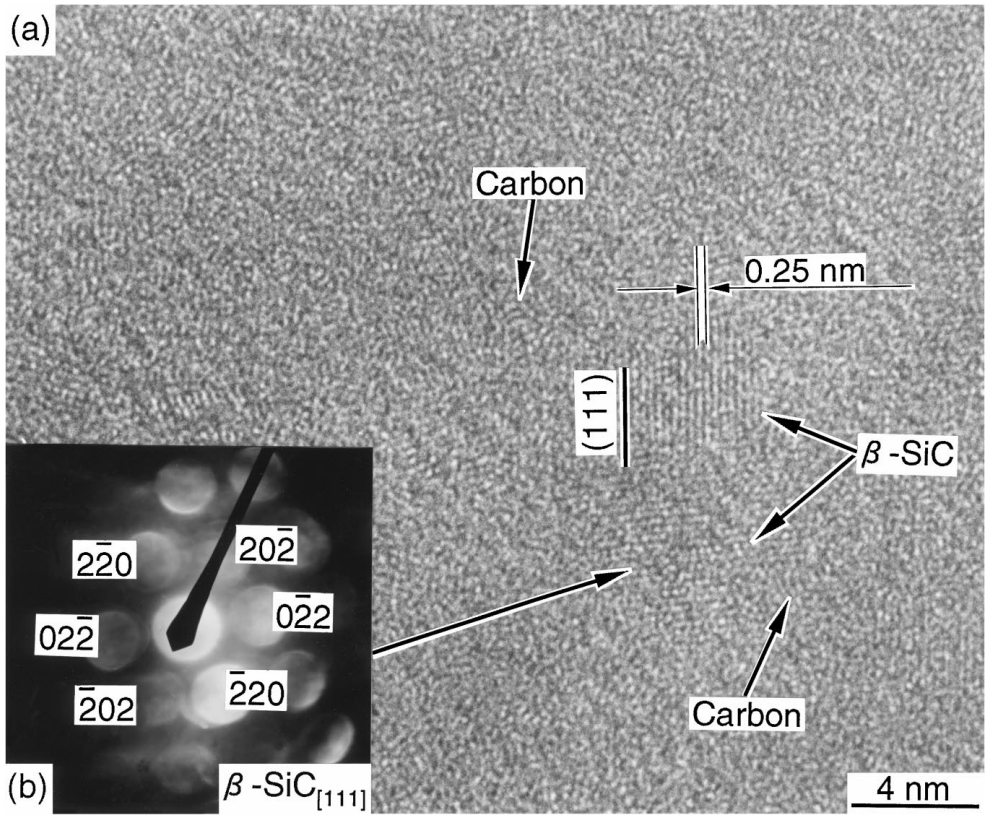

Figure 2 (a) HRTEM image of an as-received fiber, showing the β-SiC, free carbon and intergranular phase, (b) CBED pattern of β-SiC$_{(111)}$.

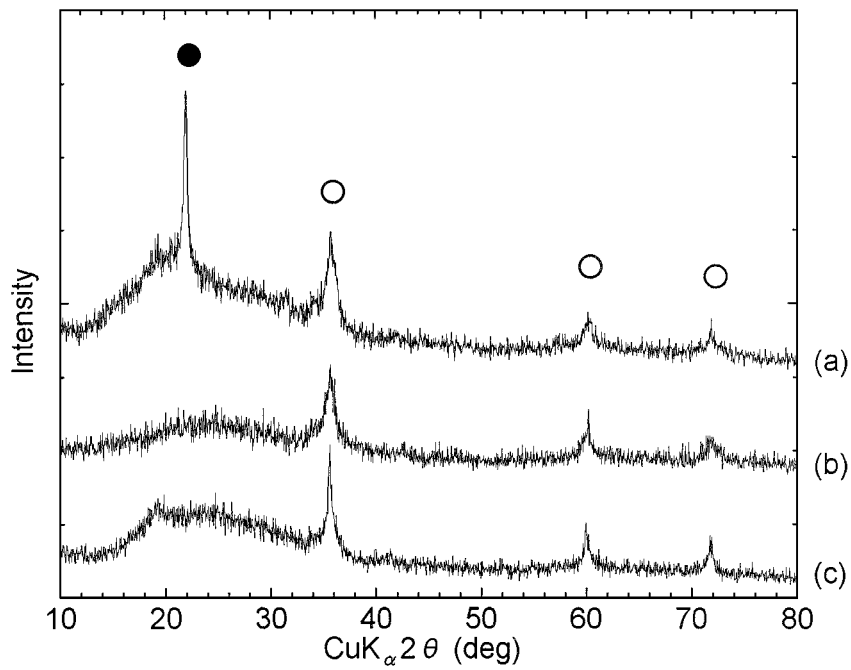

Figure 3 X-ray diffraction patterns of annealed fibers in air (a), an argon flow (b) and an ultra high-purity argon flow (c); ○ and ● refer to β-SiC and α-SiO_2, respectively.

conducted in an alumna tube with a length of 1000 mm. The hot zone in which the temperature deviation is lower than 10 °C was about 50 mm in length. The fibers analyzed were tested in the hot zone.

In the annealing, fibers of 20 mm in length were placed in an alumna boat and heated at 1500 °C. The desired heat-treatment temperature was reached within 15 h, and after 1 h of soaking, the fibers were furnace-cooled. Static air, a commercial grade argon flow, and an ultra high-purity argon flow (4.2 l/h) were used as the annealing atmospheres, in which the oxygen contents were 21%, 1.0 ppm and 0.1 ppb, respectively. The water steam in the argon flow was not inspected. Creep tests were conducted on fibers in the form of yarn in the same atmospheres and at the heating temperature as those used in the annealing treatments. The creep load, which was applied by hanging a load cell on one end of a yarn while fixing the other end, was 95 g/yarn.

Elemental analysis of the as-received fibers was performed on fiber cross-sections by electron-probe microanalysis (EPMA). The phases existing in the fibers were identified using an X-ray diffractometer. The average grain size was then calculated from the half-value width of the peak by employing the Scherrer formulation. The morphologies of the fiber surface and cross section were characterized using SEM. TEM observations and high resolution image were preformed using a JEOL 2010FE operated at 200 keV and equipped with a thin-window energy-dispersive spectroscope (EDS). TEM samples were prepared by using the focused ion beam thinning method (FIB). As-received fibers and tested fibers were cut to 3 mm in length and glued on half copper rings of 3 mm in diameter. In order to preserve the structure of the fiber surface, tungsten deposition on the fiber surface was performed before ion thinning.

3. Experimental results

3.1. Properties of as-received fiber

The average bulk compositions of the as-received fiber measured by EPMA techniques are shown in Table I. There were a slight differences between the EPMA results and the manufacturer's reported data, which probably resulted from processing variations. The oxygen content of Hi-Nicalon^{TM} was very low compared to oxygen-cured Nicalon fibers. The C : Si ratio (C : Si = 1.2) showed that Hi-Nicalon^{TM} fiber contains about 16.5 at% free carbon.

Fig. 2a is a HRTEM image of the as-received fiber. The as-received fiber was composed of silicon carbide, free carbon and an intergranular phase. The lattice parameter of the silicon carbide, 0.25 nm, was identified as {111} planes of the β-SiC crystal. A convergent beam electron diffraction (CBED) pattern obtained from a silicon carbide crystal also verified that the silicon carbide was β-SiC (Fig. 2b). The total volume of the β-SiC phase could be extrapolated in the order of 70–80% from the TEM image. The average grain size of β-SiC measured by XRD was about 5 nm. Free carbon was stacked by slightly distorted carbon layers with a length of 1 nm. The intergranular phase was an

TABLE I Composition of as-received Hi-Nicalon^{TM} fiber measured by EPMA

		Si	C	O	C/Si
Hi-Nicalon^{TM}	at %	45.2	54.1	0.7	1.2
	wt%	65.7	33.7	0.6	
Nicalon[a]	at%	37.4	49.0	13.58	1.2
	wt%	56.6	31.7	11.7	

[a]Reported by the manufacture.

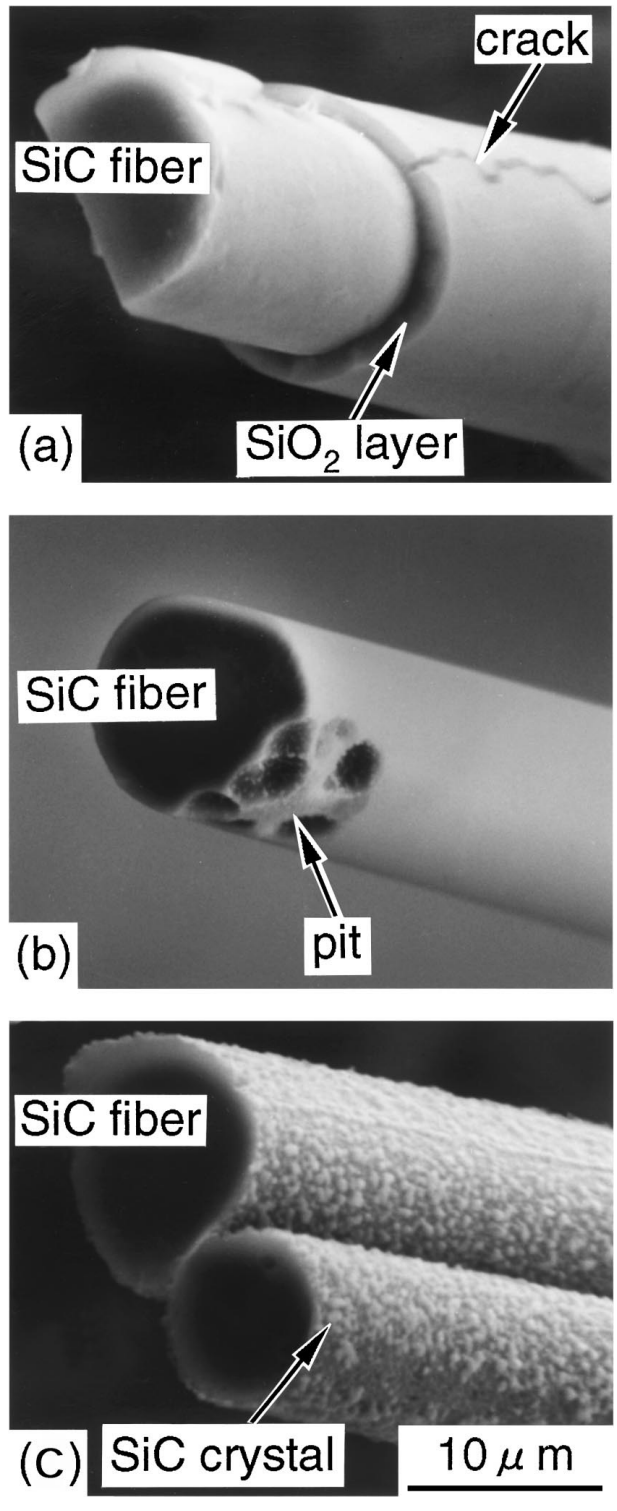

Figure 4 Morphologies of fibers annealed in air (a), an argon flow (b) and an ultra high-purity argon flow (c).

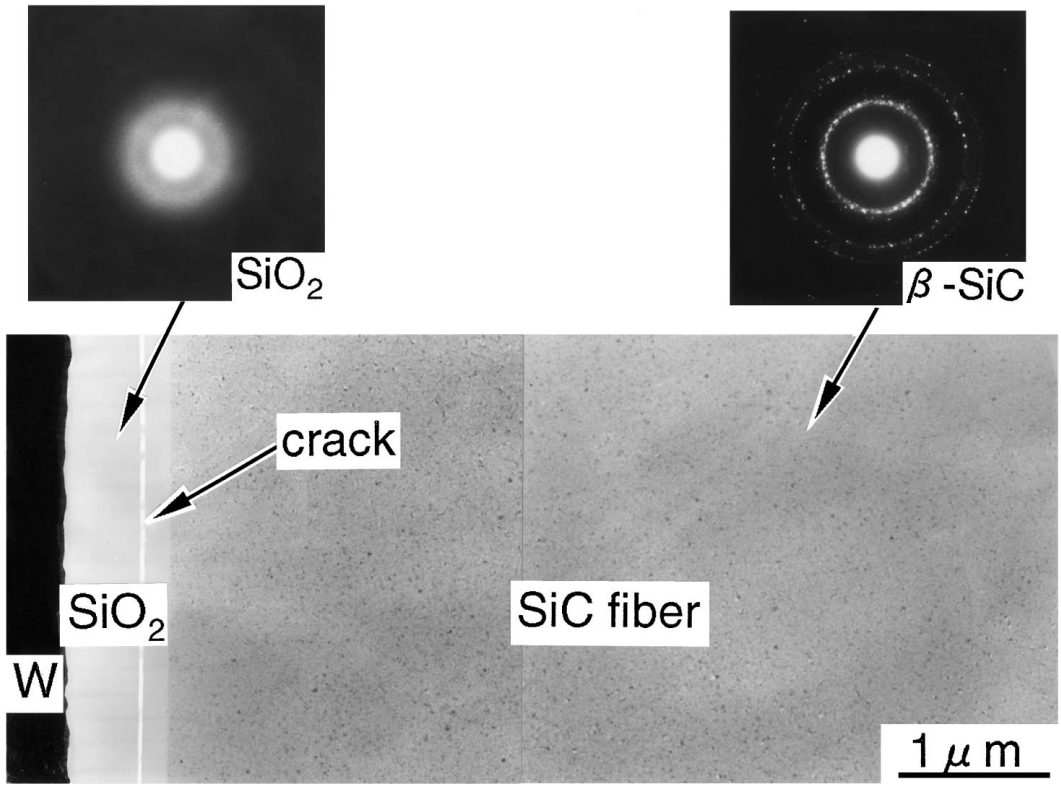

Figure 5 Cross sectional TEM image and electron diffraction patterns of a fiber annealed in air.

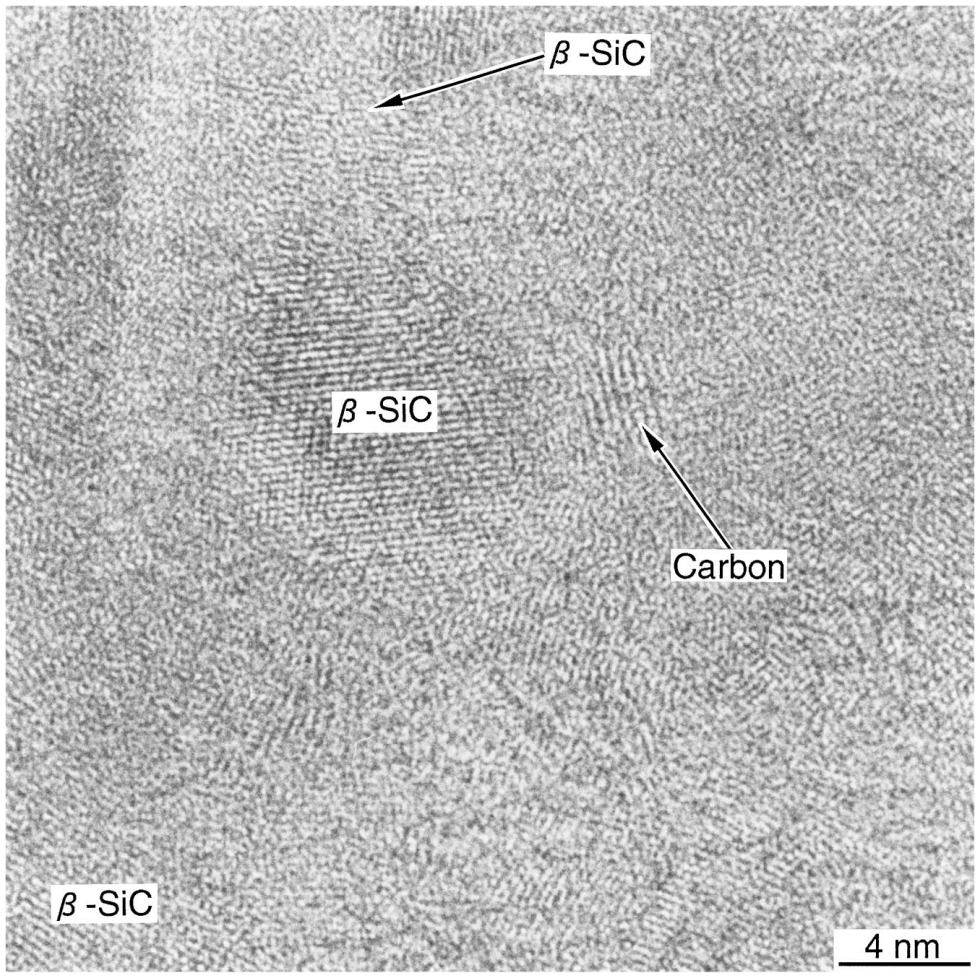

Figure 6 HRTEM image of a fiber annealed in air.

amorphous silicon oxycarbide phase (SiO_xC_y). The very low oxygen content of the Hi-Nicalon^{TM} fibers implied a low percentage of the intergranular phase in the fibers. The intergranular phase decomposed with evaporation of gaseous SiO and CO at a temperature above 1000 °C, as shown by the follow equation [3–7, 13, 14, 16].

$$SiO_xC_y(s) \rightarrow SiC(s) + C(s) + SiO(g) + CO(g) \quad (1)$$

3.2. Results of annealing treatments

3.2.1. X-ray diffraction profile

The Hi-Nicalon^{TM} fibers were oxidized at high temperature heat treatment in air atmosphere. As shown in Fig. 3, besides β-SiC peaks, silica peaks also existed in the X-ray diffraction pattern obtained from the fibers annealed in air, unlike in the patterns obtained from the fibers annealed in an argon flow or in an ultra high-purity argon flow. The silica was identified as α-cristobalite. On the other hand, the β-SiC peaks became sharper with decreases in the oxygen content of the atmosphere. The average β-SiC grain sizes of the annealed fibers were 7.7 nm in air, 8.2 nm in argon flow and 12.6 nm in ultra high purity argon flow.

3.2.2. Morphology

SEM micrographs of the annealed fibers are shown in Fig. 4. Oxidized fibers were surrounded by a silica layer (Fig. 4a). This silica layer, which had a smooth surface, consisted of a concentric debonded sheath. Cracks had also formed within the silica layer. After being annealed in an argon flow, most of the fiber surface had retained its original morphology and only a few pits created in the fiber surface made the fiber slightly degraded (Fig. 4b). Pits occurred from surface flaws probably induced by fiber processing. In an ultra high-purity argon flow, crystals was observed on the fiber surface (Fig. 4c). From TEM inspections lately, they were confirmed to be β-SiC crystals.

3.2.3. Microstructure analysis

3.2.3.1. Fiber annealed in air. Fig. 5a shows a TEM micrograph of the fiber annealed in air. Cracks were distributed inside the silica layer, and the inner silica layer was adjacent to the bulk of the fiber. Broadening of continuous rings in the electron diffraction of the silica layer indicated that the silica was crystalline α-cristobalite (Fig. 5b). Because of the lower thermal expansion of SiO_2 compared to SiC, cracks in the silica layer resulted from the different thermal expansion in the bulk fiber and the silica, which put the silica layer in tension on cooling [17]. The electron diffraction pattern of bulk fiber shows three main rings, corresponding to the 111, 220 and 311 β-SiC Bragg reflections (Fig. 5c). These rings were sharp and split, which is consistent with the relatively larger size of the crystals. The growth of both grains, β-SiC and free carbon, was revealed in high resolution image (Fig. 6). It was easier observed the region with the continuum of SiC grains and better organized free carbon grains.

3.2.3.2. Fiber annealed in an argon flow. Fig. 7 is a TEM micrograph recorded near the fiber surface. An amorphous layer of about 80 nm in thickness formed

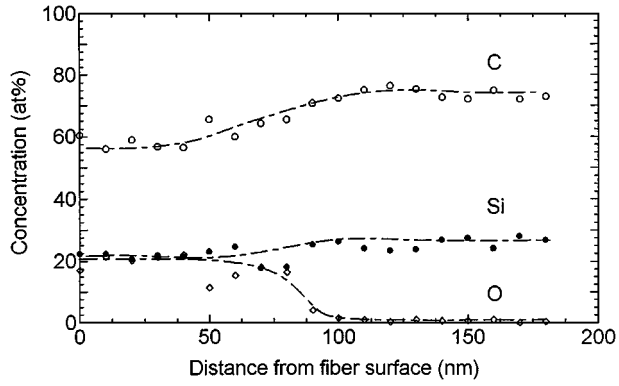

Figure 8 EDS results of a fiber annealed in an argon flow.

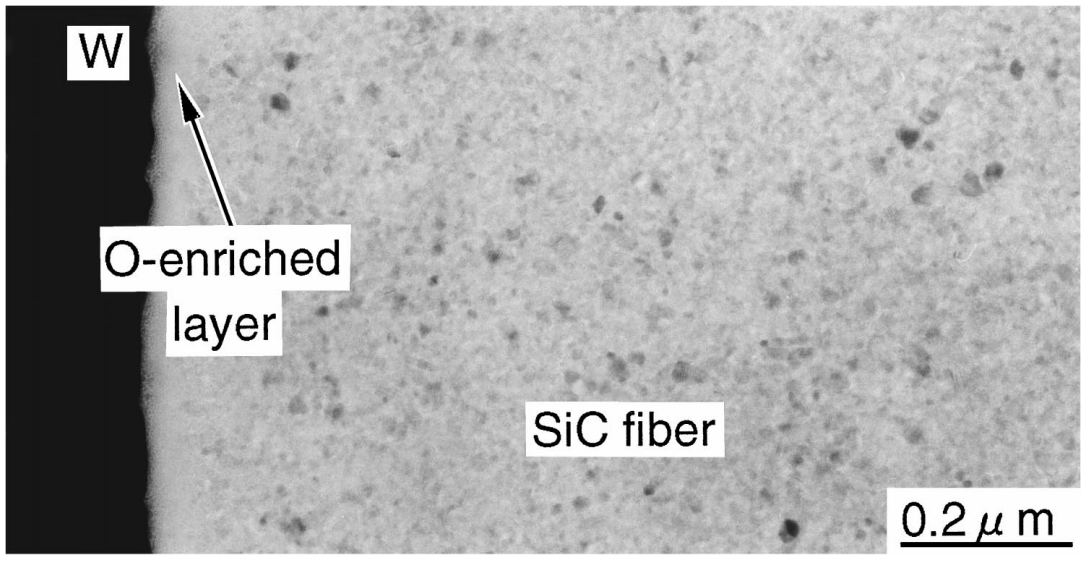

Figure 7 Cross sectional TEM image of a fiber annealed in an argon flow.

on the skin of the fiber; this was not found in the as-received fiber by TEM. The compositions near the fiber surface measured by EDS analysis, as shown in Fig. 8, indicated that the mole ratio of silicon to carbon was constant and that the oxygen content in the amorphous layer was higher than that in the bulk fiber. Oxygen-enriched thin film on the surface of a Hi-Nicalon^{TM} fiber has been analyzed using an Auger electron spectroscope (AES), and it was reported that the film, which is about 5 nm in thickness, seems to be attributable to the fiber fabrication processing [11]. In this study, however, the oxygen-enriched layer on the annealed fibre surface was found to be thicker than that on the surface of Hi-Nicalon^{TM} fiber, indicating the existence

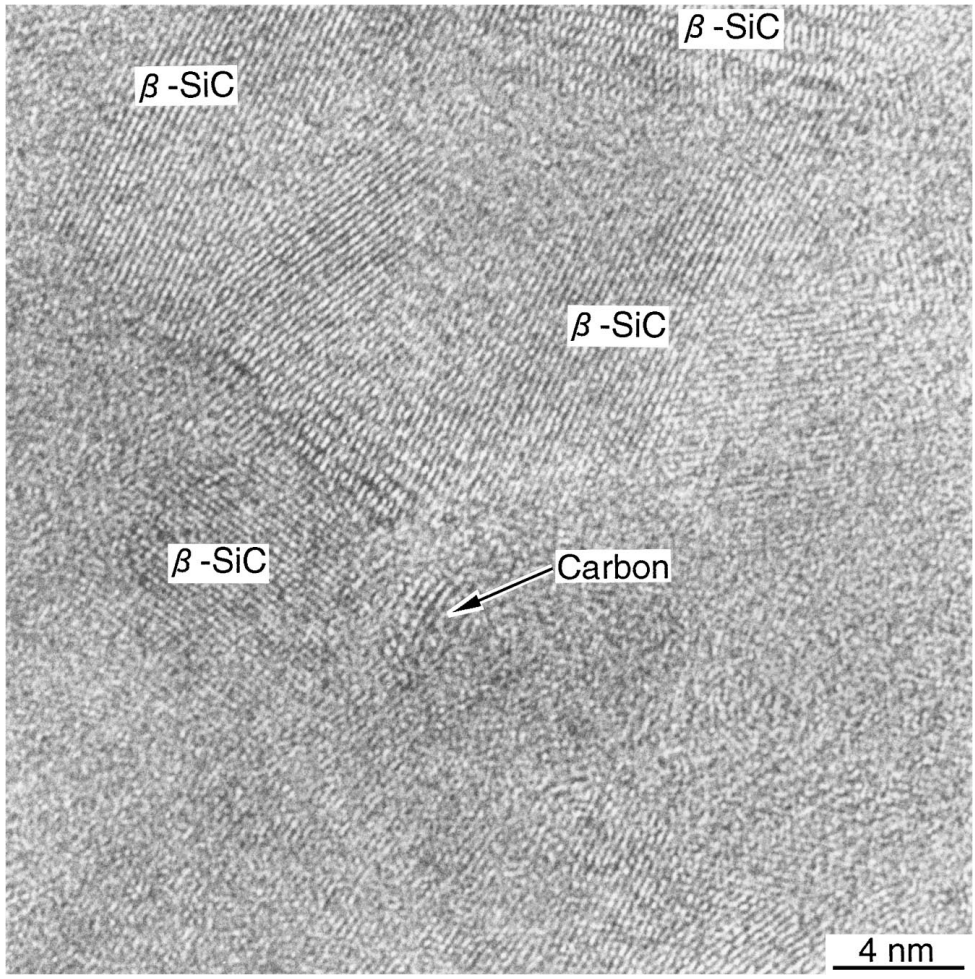

Figure 9 HRTEM image of a fiber annealed in an argon flow.

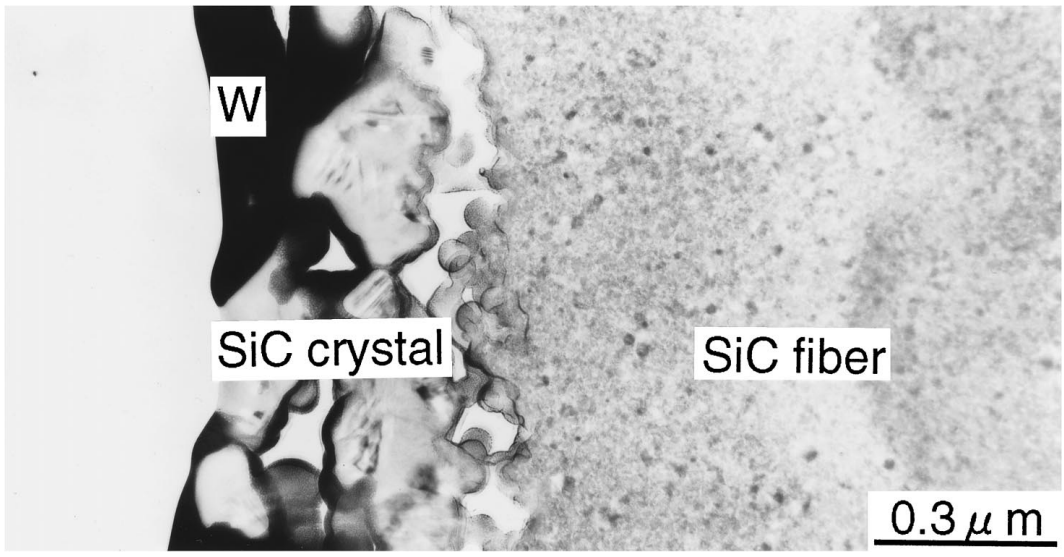

Figure 10 Cross sectional TEM image of a fiber annealed in an ultra high-purity argon flow.

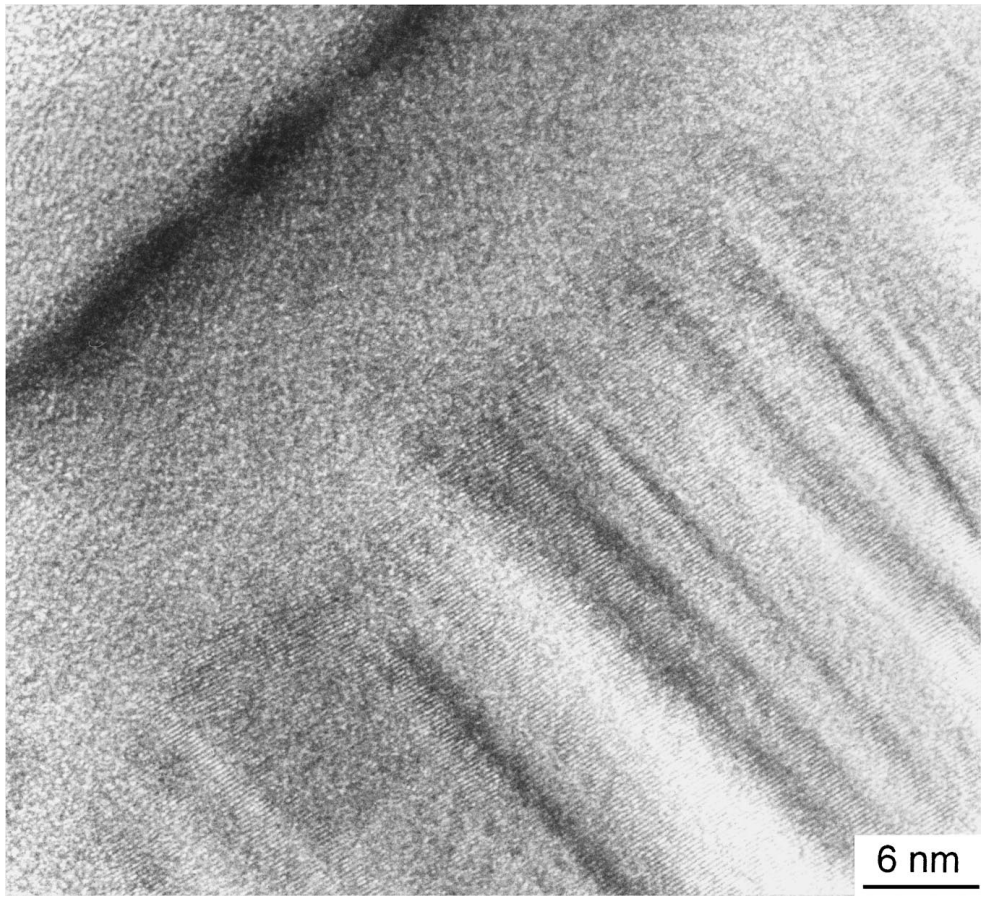

Figure 11 HRTEM image of a SiC crystal on the fiber surface in an ultra high-purity argon flow.

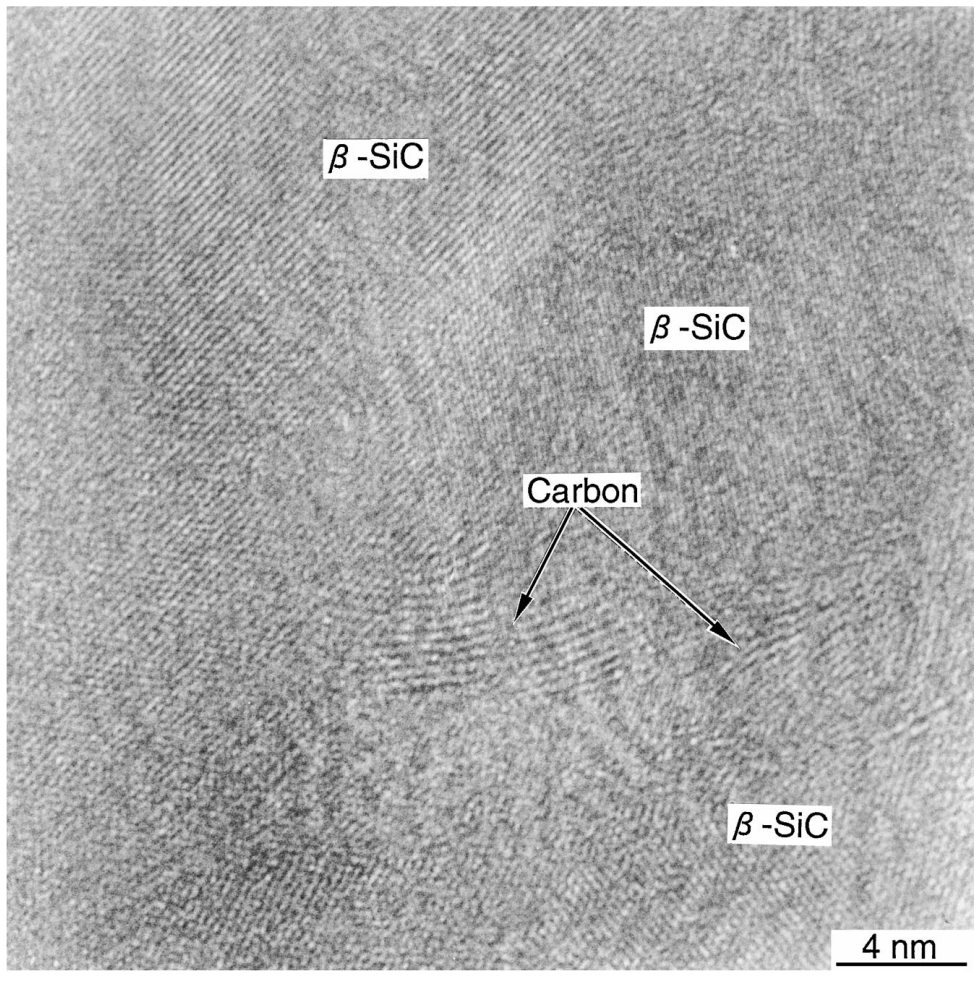

Figure 12 HRTEM image of a fiber annealed in an ultra high-purity argon flow.

of another mechanism of oxygen-enriched layer formation. Similar to the fiber after being annealed in air, the continuum of lattice-imaged SiC grains and narrow intergranular phase revealed growth of the grain (Fig. 9).

3.2.3.3. Fiber annealed in an ultra-high purity argon flow. The microstructure of crystals on fiber the surface is shown in Fig. 10. Those crystals grew outward from the fiber surface, and the thickness of the crystals was 0.5 μm. Part of the crystal was inlaid in the fiber and the main part of the crystal was free. The crystals were identified as β-SiC by high resolution TEM inspection, and they contained some stack faults (Fig. 11). Since SiO and CO gases evolved together with the growth and coarsening of SiC grain when the fiber was annealed at a high temperature due to decomposition of the amorphous intergranular phase, it was thought that SiC crystals were produced by the following chemical reaction between SiO and free C on the skin of the fiber:

$$SiO + 2C \rightarrow SiC + 2CO. \quad (2)$$

A high resolution micrograph of the fiber is shown in Fig. 12. It reveals the SiC grain and free carbon grew more. Moreover, free carbon was distributed along the SiC grain boundary.

3.3. Results of creep tests

3.3.1. X-ray diffraction profiles

X-ray diffraction patterns of the crept fibers are shown in Fig. 13. The silica peaks in the diffraction patterns of the fiber crept in air were more intense compared with those in diffraction patterns obtained from the fiber annealed in air. In addition, the average grain sizes of β-SiC in the fibers crept in air, in an argon flow and in ultra high purity argon flow were 14.3 nm, 20.3 nm and 20.3 nm, respectively. A comparison of the average grain sizes in fibers that had been creep tested and those that had been annealed in the same atmospheres showed the creep load enhanced the growth of the SiC grains.

3.3.2. Morphology

SEM micrographs of the crept fibers are shown in Fig. 14. After the fiber was crept in air, a porosity silica layer with a rough surface and cracks was formed on the fiber surface. The silica layer was about three-times thicker than that formed on the surface of the fiber annealed in air; moreover, the SiC was thinner due to severe oxidation of the fiber under the creep load. In the cases of creeping fiber in an argon flow and in an ultra high purity argon flow, the SiC crystals grew outward on the fiber surfaces.

3.3.3. Microstructure analysis

3.3.3.1. Fiber crept in air. A TEM micrograph revealed that the pores distributed throughout the silica layer and the pores near the silica-SiC fiber interface were smaller than those in other places. (Fig. 15a). The formation of pores seem to be due to the production of gases that evolved from the reaction between oxygen in air and SiC [12]. Cracks also formed in the silica layer. SAD analysis of the silica layer indicated that the silica completely crystallized under the creep load (Fig. 15b). On the other hand, the SAD pattern in bulk fiber appeared sharper compared with that in air-annealed fiber, indicating that enhanced grain growth occurred under the

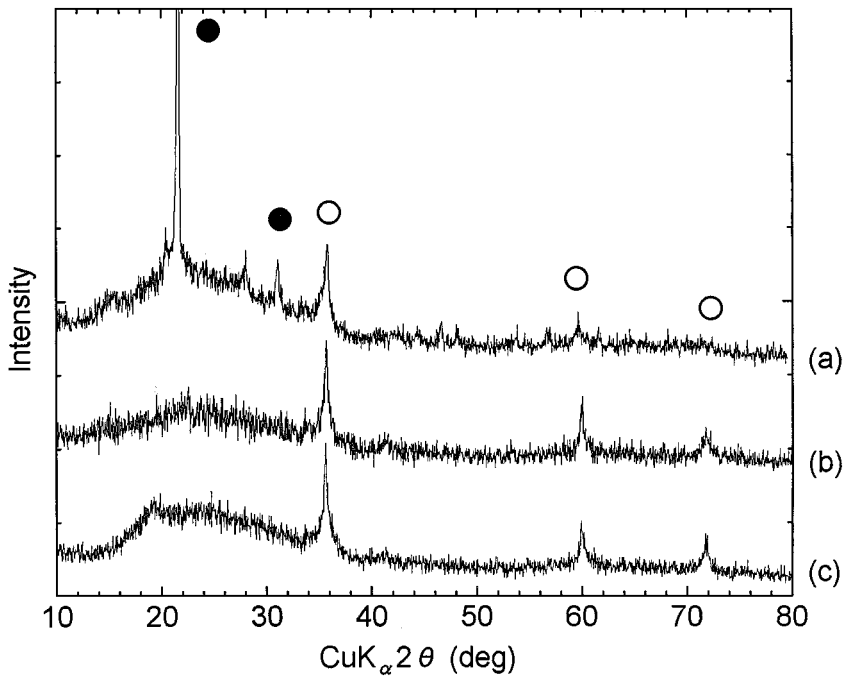

Figure 13 X-ray diffraction patterns of crept fibers in air (a), an argon flow (b) and an ultra high-purity argon flow (c); ○ and ● refer to β-SiC and α-SiO_2, respectively.

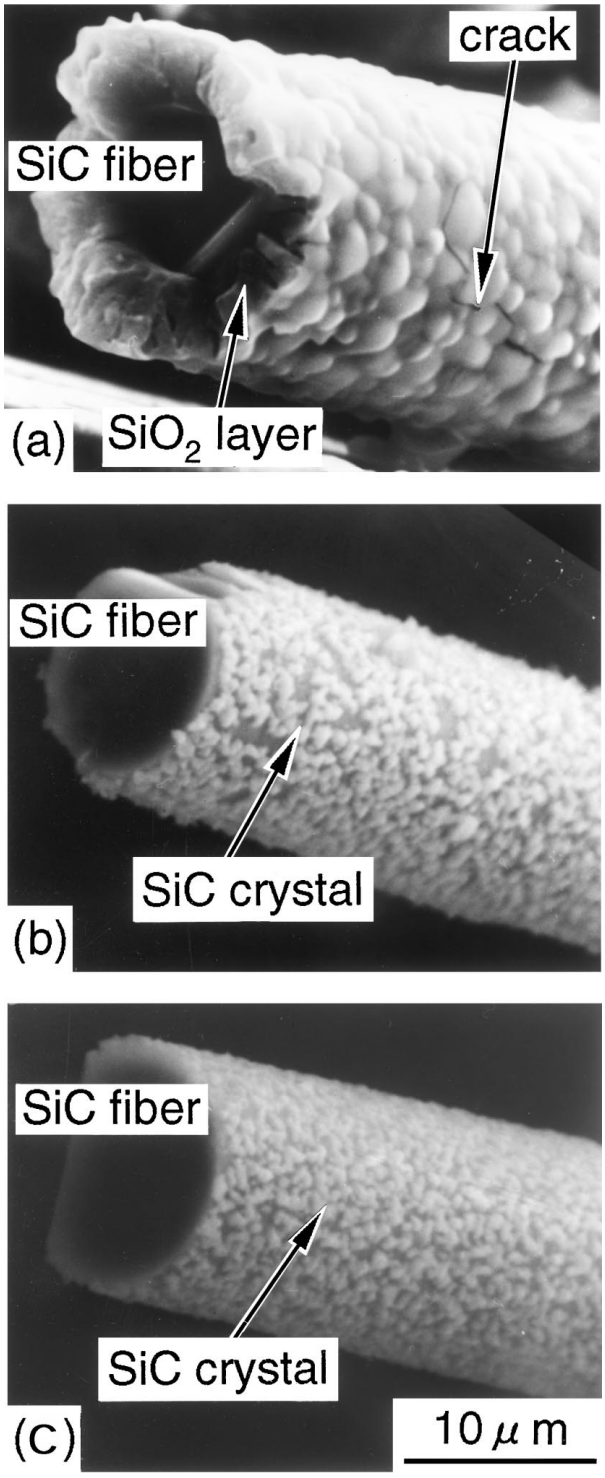

Figure 14 Morphologies of fibers crept in air (a), an argon flow (b) and an ultra high-purity argon flow (c).

creep load, which is consistent with the results quantified from XRD (Fig. 15c).

Fig. 16 shows a HRTEM image near the fiber-silica interface. Some residual SiC grains were distributed in the silica layer; these were not to found in the fiber annealed in air. Therefore, it is thought that cracks formed under creep load due to stress corrosion and crystallization of the silica phase when the fiber was heating. The oxidation mechanism is transportation of oxygen molecules through the cracks, which is different from the oxidation mechanism in the case of annealing in air, i.e., is lattice diffusion of ionic oxygen [18]. The oxidation of SiC fiber near the cracks was rapider than that in the other parts due to the high oxygen potential in the cracks, and resulted in some residual SiC grains were found in the silica layer.

3.3.3.2. Fiber creep tested in an argon flow. When the fiber was annealed in an argon flow, an oxygen-enriched layer formed on the surface of the fiber, whereas in the case of creep testing the fiber in an argon flow, SiC crystals grew outward on the fiber surface, as shown in Fig. 17. It is thought that stress corrosion cracking was generated on the thin silica film when the creep load was applied. SiO and CO gases were transported through the cracks, and SiC crystals were produced by a chemical reaction between SiO and free C on the skin of the fiber.

3.3.3.3. Fiber creep tested in an ultra-high purity argon flow. A TEM micrograph of the fiber is shown in Fig. 18. The SiC crystal layer in the case of creep testing the fiber in an ultra-high purity argon flow had a thickness of about 1.4 μm and was the thickest of all cases. This indicates that more SiO gases were generated due to the enhanced grain growth. Therefore, more SiC crystals grew on the surface due to the chemical reaction, as shown in Equation 2.

4. Discussion

4.1. Passive and active oxidation

Generally, the oxidation behavior of silicon carbide at a high temperature depends on ambient oxygen partial pressure. The thermochemical correlation for active and passive oxidation of silicon carbide is shown in Fig. 19 [19]. The line shows the equilibrium pressure of O_2, SiO and CO. In the region above the line, the reaction is passive oxidation, which means the silicon carbide will be oxidized. In the region below the line, the reaction is active oxidation, which means the silica will be decomposed. Therefore, the Hi-Nicalon fibers were oxidized in air atmosphere and decomposed in an ultra-high purity argon flow. In an argon flow, however, the fibers were oxidized in the annealing treatment and decomposed in the creep test. Because an alumna tube was used in the annealing and a water stream was probably contained in the argon flow, the real oxygen partial pressure is higher than the equilibrium pressure. A thin silica film formed on the fiber surface and prevented SiO and CO gases from passing through the fiber surface. An oxygen-enriched layer was therefore formed near the fiber surface. Under a load, the growth of β-SiC and decomposition of the amorphous intergranular phase were enhanced. In this case, the pressure of SiO and CO gas increased. The oxidation changed from passive to active. The thin silica film was removed by active oxidation. While the SiO and CO gases were transported through the fiber surface, SiC crystals grew on the fiber surface due to the reaction between SiO and free carbon.

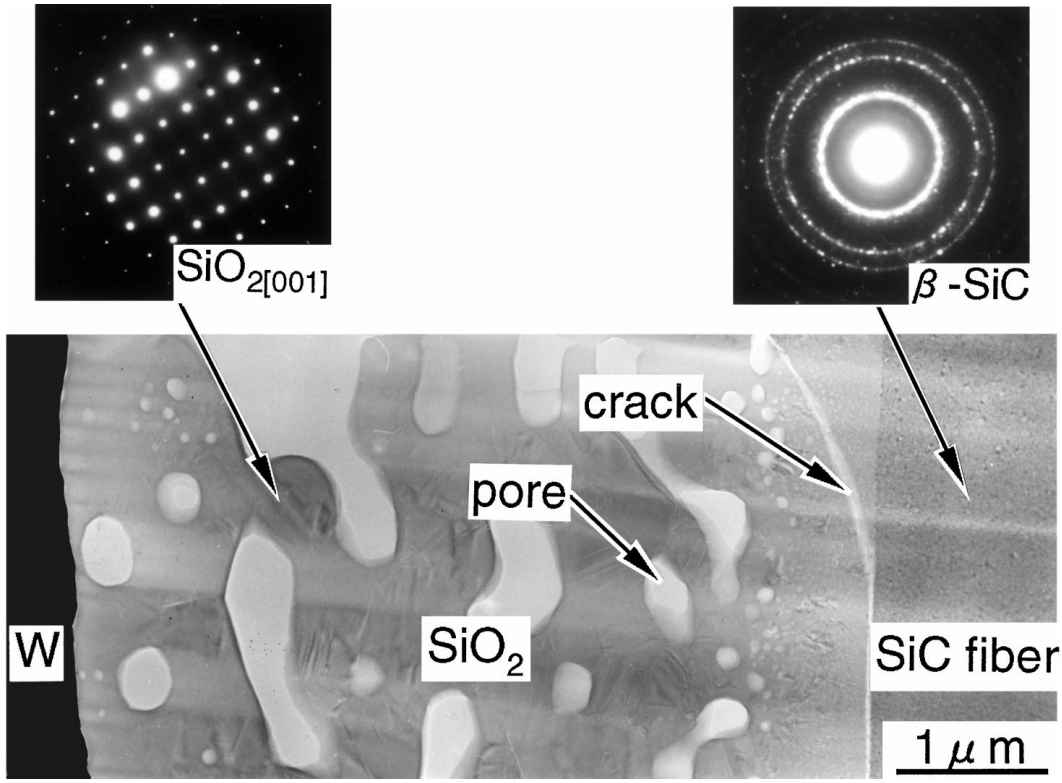

Figure 15 Cross sectional TEM image and electron diffraction patterns of a fiber crept in air.

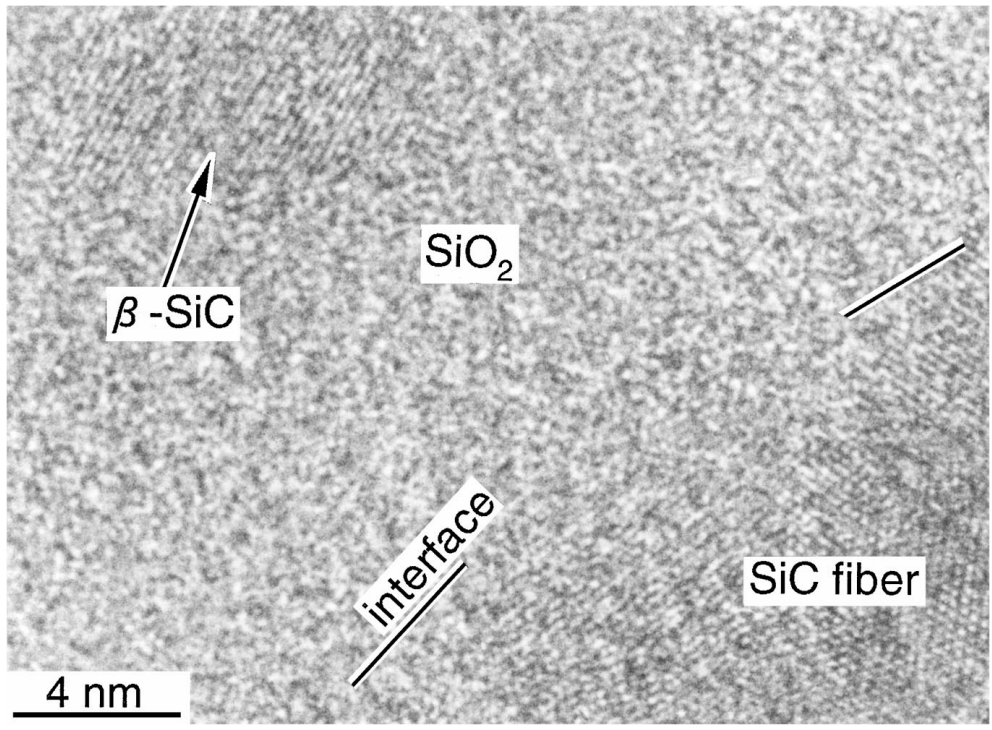

Figure 16 HRTEM image showing the SiC/SiO_2 interface of a fiber crept in air.

4.2. Grain growth in annealed and crept fibers

The average grain sizes in the annealed and crept fibers are shown in Fig. 20. The SiC grain size increased with decreases in the ambient oxygen partial pressure in the same treatments. This phenomena can be explained by the morphology of the fiber surface, because grain growth was accompanied by the generation of SiO and CO gases, and the grain growth was controlled by the transportation of SiO and CO gas through the fiber surface. In the case of high oxygen partial pressure, a silica layer formed on the fiber surface and prevented the SiO and CO gases from passing through the fiber surface. Therefore, the growth of SiC grain was restrained. On

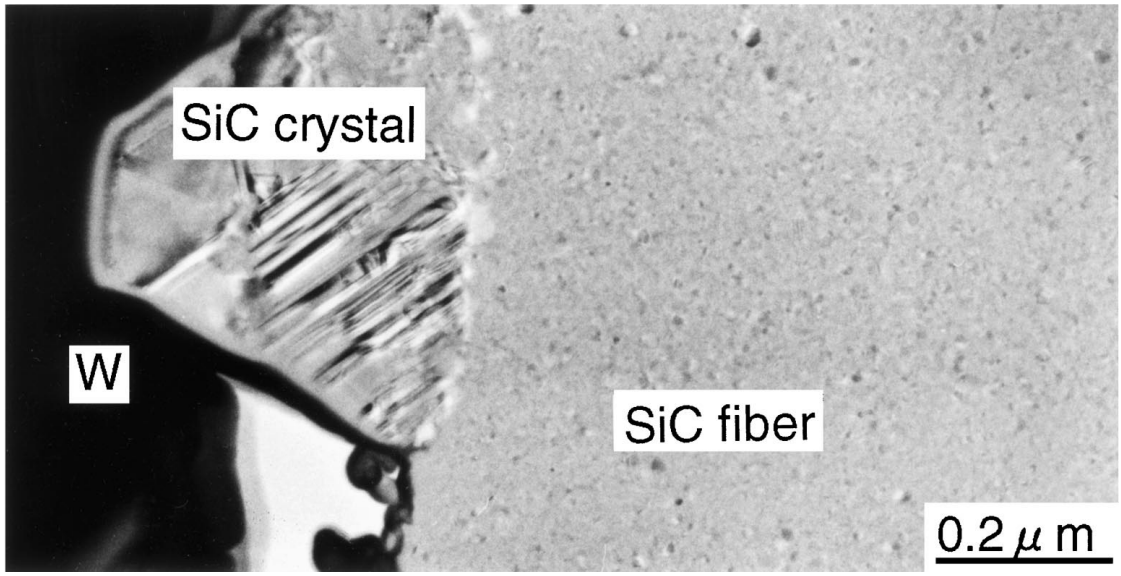

Figure 17 Cross sectional TEM image of a fiber crept in an argon flow.

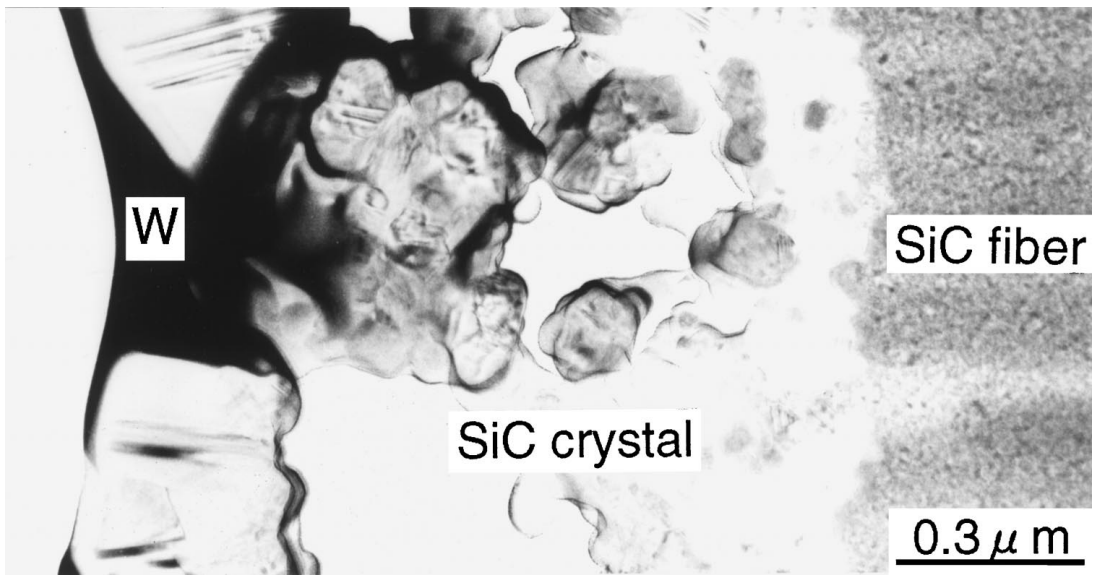

Figure 18 Cross sectional TEM image of a fiber crept in an ultra high-purity argon flow.

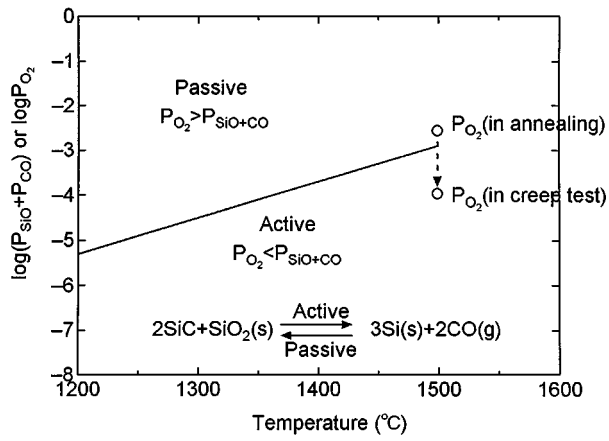

Figure 19 Thermochemical correlation for active and passive oxidation of silicon carbide in an argon flow.

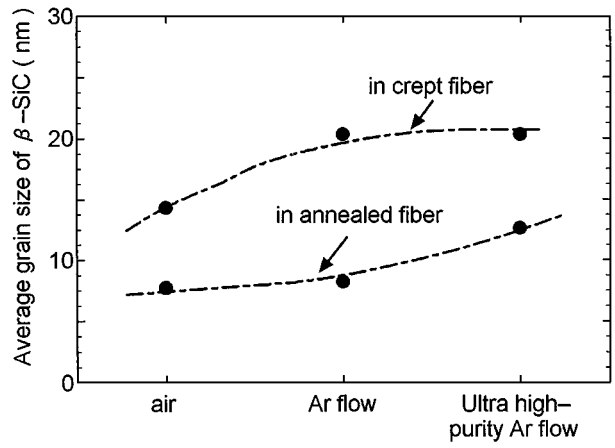

Figure 20 Comparsion of the average β-SiC grain sizes in annealed and crept fibers.

the other hand, in ultra low oxygen partial pressure, no silica layer was formed to prevent the gases from passing through the fiber surface, allowing the SiC grain to grow.

Compared to annealed fibers, the grain size was bigger in the case of crept fiber. The growth and coarsening of SiC in bulk fiber were enhanced in the case of the creep test. It is thought that the stress induced the grain growth by reducing the activation energy.

5. Conclusion

The structural evolution of Hi-Nicalon^{TM} SiC fiber as a function of oxygen partial pressure and load condition was investigated. The follow conclusions were drawn from the results.

1. A silica layer with cracks formed on the fiber surfaces after the annealing treatment and the creep test in air. In the case of annealing, the cracks occurred on cooling, while the cracks occurred on heating and the silica layer was thicker due to transportation of oxygen to bulk fiber through the cracks in the case of the creep test.

2. During annealing in an argon flow, the fiber slightly decomposed, and decomposition under creep load was caused by removal of the protective thin silica film on the fiber surface due to active oxidation.

3. The fibers decomposed during the annealing treatment and creep test in an ultra high-purity argon flow, and SiC crystals grew on the fiber surface due to the reaction between SiO gas and free carbon.

References

1. S. YAJIMA, J. HAYASHI and M. OMORI, *Chem. Lett.* **9** (1975) 931.
2. *Idem., ibid.* **10** (1976) 551.
3. T. MAH, N. L. HECHT, D. E. MCCULLUM, J. R. HEONIGMAN, H. M. KIM, A. P. KATZ and H. A. LIPSITT, *J. Mater. Sci.* **19** (1984) 1191.
4. S. M. JOHNSON, R. D. BRITTAIN, R. H. LAMOREAUX and D. J. ROWCLIFFE, *J. Amer. Ceram. Soc.* **71** (1988) C132.
5. D. J. PYSHER, K. C. GORETTA, R. S. HODDER and R. E. TRESSLER, *ibid.* **72** (1989) 284.
6. T. SHIMOO, M. SUGIMOTO and K. OKAMURA, *J. Jap. Inst. Metals* **54** (1990) 802.
7. T. SHIMOO, H. M. CHEN and K. OKAMURA, *J. Ceram. Soc. Japan* **100** (1992) 48.
8. K. OKAMURA, *Composites* **18** (1987) 107.
9. M. TAKEDA, Y. IMAI, H. ICHIKAWA, T. SEGUCHI and K. OKAMURA, *Ceram. Eng. Sci. Proc.* **12** (1991) 1007.
10. *Idem., ibid.* **13** (1992) 209.
11. T. SHIMOO, T. HAYASTU, M. NARISAWA, M. TAKEDA, H. ICHIKAWA, T. SEGUCHI and K. OKAMURA, *J. Ceram. Soc. Japan.* **101** (1993) 1379.
12. G. CHOLLON, R. PAILLER, R. NASLAIN, F. LAANANI, M. MONTHIOUX and P. OLRY, *J. Mater. Sci.* **32** (1997) 327.
13. T. SHIMOO, I. TSUKADA, T. SEGUCHI and K. OKAMURA, *J. Amer. Ceram. Soc.* **81** (1998) 2109.
14. R. BODET, X. BOURRAT, J. LAMON and R. NASLAIN, *J. Mater. Sci.* **30** (1995) 661.
15. N. HOCHET, M. H. BERGER and A. R. BUNSELL, *J. Microsc.* **185** (1997) 243.
16. K. L. LUTHRA, *J. Amer. Ceram. Soc.* **69** (1988) C-231.
17. V. PAREEK and D. A. SHORES, *ibid.* **74** (1991) 556.
18. J. A. COSTELLO and R. E. TRESSLER, *ibid.* **69** (1986) 674.
19. E. A. GULBRANSEN and S. A. JANSSON, *Oxid. Of Met.* **4** (1972) 181.

Received 3 March
and accepted 16 August 1999